ANALYTIC DESCRIPTION OF THE NOISE RADIATION FROM SINGLE- AND CONTRA-ROTATING PROPELLERS

H. Brouwer
National Aerospace Laboratory NLR

Keywords: *propulsion, propellers, noise*

Abstract

Analytical expressions are presented for the radiation of noise from single- and contra-rotating propellers. These expressions can be used to assess which design and operational parameters have the largest effect on the noise radiation efficiency of such propulsion systems. An analysis of the directivity of the individual noise components is given. Furthermore, it is shown how the mathematical model enables an exact extrapolation of near-field noise data to the far field.

1 Introduction

Because of the growing concern on CO2 emissions, and because of the expectation that fuel prices will increase considerably in the long term, the aircraft industry is diligently searching for high efficiency propulsion systems for the next generation short-to-medium haul aircraft. A propulsion system that offers the prospect of being much more efficient than todays turbofan engines, is the contra-rotating open rotor (or contra-rotating propeller). Preliminary estimates amount to a reduction in fuel consumption of 20 to 25%. An example of such a propulsion system is General Electric's Unducted Fan, which was tested in the late 1980's, see fig.1.

Fig. 1. GE's Unducted Fan

However, because the rotor is not shielded from the ambient air by a nacelle, the noise radiated by an open rotor is considered as a potential problem, which may be an obstacle to achieve the aviation industry's equally challenging targets on noise reduction.

Therefore, it is necessary to assess the noise generation during the design of contra-rotating propellers. A final assessment will in practice be done by acoustic wind tunnel tests on a model and, eventually, by flight-testing of a prototype, but these tests are obviously too expensive to be carried out for parametric studies during initial designs. In principle, the noise can be computed for a given geometry by using CFD and CAA tools, but such computations are also quite expensive and time consuming. Besides, the application of such tools to contra-rotating propellers is not a proven technology yet. To date, no experimental validation of these tools has been published yet.

Thus the need exists for analytical tools, which can be used for an early optimization of propeller designs, and for the analysis and extrapolation of data obtained from earlier test activities on similar systems.

2 Mathematical model

2.1 Single-rotating propeller

In the following analysis we consider a single rotating propeller with B blades, rotating with angular speed Ω, in a uniform flow parallel to the propeller axis, for which we take the x-axis. In that case the equation for the acoustic pressure can be written as:

$$\left(\frac{1}{c_0^2}\left(\frac{\mathrm{D}}{\mathrm{D}t}\right)^2-\nabla^2\right)p=Q(x,r,\theta-\Omega t) \qquad (1)$$

where a cylindrical coordinate system is assumed. $\frac{\mathrm{D}}{\mathrm{D}t}$ is the material derivative $\frac{\mathrm{D}}{\mathrm{D}t}=\frac{\partial}{\partial t}+U\frac{\partial}{\partial x}$, with U the ambient flow velocity.

The source Q depends on the aerodynamic forces on the propeller blades, and is not specified any further. We do know however that Q is periodical in θ with period $2\pi/B$, and is limited to the propeller disc:

$$\begin{aligned} &Q(x,r,\theta-\Omega t)=Q(x,r,\theta-\Omega t+\frac{2\pi j}{B}), \quad j=1,2,...B\\ &Q(x,r,\theta-\Omega t)=0, \quad r>R \end{aligned} \qquad (2)$$

where R is the propeller radius. The periodicity allows us to write:

$$Q(x,r,\theta-\Omega t)=\sum_{n=-\infty}^{\infty}\hat{Q}_n(x,r)e^{inB(\theta-\Omega t)} \qquad (3)$$

As the resulting pressure field has the same periodicity, we write the solution as:

$$p(x,r,\theta,t)=\sum_{n=-\infty}^{\infty}\hat{p}_n(x,r)e^{inB(\theta-\Omega t)} \qquad (4)$$

The n-th component of the equation becomes:

$$\left[\frac{\partial^2}{\partial r^2}+\frac{1}{r}\frac{\partial}{\partial r}-\frac{(nB)^2}{r^2}+\frac{\partial^2}{\partial x^2}+\left(\frac{nB\Omega}{c_0}+iM\frac{\partial}{\partial x}\right)^2\right]\hat{p}_n(x,r)=\hat{Q}_n(x,r) \qquad (5)$$

with $M = U/c_0$. We now define:

$$\tilde{p}_n(\alpha,r)=\int_{-\infty}^{\infty}e^{-i\alpha x}\hat{p}_n(x,r)\,\mathrm{d}x \qquad (6)$$

and similar for Q, and take the Fourier transform of eq.(5):

$$\left[\frac{\partial^2}{\partial r^2}+\frac{1}{r}\frac{\partial}{\partial r}-\frac{(nB)^2}{r^2}-\alpha^2+\left(\frac{nB\Omega}{c_0}-M\alpha\right)^2\right]\tilde{p}_n(\alpha,r)=\tilde{Q}_n(\alpha,r) \qquad (7)$$

A Green's function satisfying the following equation is given by Schulten [1]:

$$\left[\frac{\partial^2}{\partial r^2}+\frac{1}{r}\frac{\partial}{\partial r}-\frac{m^2}{r^2}-\alpha^2+(k+M\alpha)^2\right]R_m(\alpha,r,k|\rho)=-\frac{\delta(r-\rho)}{r} \qquad (8)$$

This Green's function is expressed in Bessel functions:

$$R_m(\alpha,r,k|\rho)=-i\frac{\pi}{2}\left[J_m(\gamma r)H_m^{(2)}(\gamma\rho)\,\mathrm{H}(\rho-r)+J_m(\gamma\rho)H_m^{(2)}(\gamma r)\,\mathrm{H}(r-\rho)\right] \qquad (9)$$

with:

$$\gamma^2=(k+M\alpha)^2-\alpha^2, \quad \mathrm{Im}\,\gamma\le 0 \qquad (10)$$

See [1] on the selection of branch cuts in the complex α-plane. We thus find for $r > R$:

$$\tilde{p}_n(\alpha,r)=i\frac{\pi}{2}H_{nB}^{(2)}(\gamma r)\int_{r_h}^{R}\rho J_{nB}(\gamma\rho)\tilde{Q}_n(\alpha,\rho)\,\mathrm{d}\rho \qquad (11)$$

with r_h the hub radius and γ determined by eq.(10) and $k = -nB\Omega/c_0$. Thus:

$$\hat{p}_n(x,r)=\frac{i}{4}\int_{-\infty}^{\infty}e^{i\alpha x}H_{nB}^{(2)}(\gamma r)\times\int_{r_h}^{R}\rho J_{nB}(\gamma\rho)\tilde{Q}_n(\alpha,\rho)\,\mathrm{d}\rho\,\mathrm{d}\alpha \qquad (12)$$

This expression completes the analysis for a single-rotating propeller.

2.2 Contra-rotating propeller

In this section we consider a counter rotating propeller, with B_F front blades, rotating with angular speed Ω_F, and B_R rear blades, rotating with angular speed Ω_R, Ω_F and Ω_R having opposite sign. We will restrict the analysis to tones generated by the impingement of the wake of the front propeller on the aft blades. In practice, the noise generated by the viscous part of wakes of the front blades dominates the interaction tones.

The wakes of the front blades can be decomposed in Fourier modes, with the θ and t dependence given by:

$$e^{-inB_F(\theta-\Omega_F t)} \tag{13}$$

with n an integer.

The angular position of the j-th rear blade is given by $\theta = \Omega_R t - 2\pi j/B_R$ and the equation for the acoustic pressure can be written as:

$$\left(\frac{1}{c_0^2}\left(\frac{\mathrm{D}}{\mathrm{D}t}\right)^2 - \nabla^2\right) p = \sum_{n=-\infty}^{\infty}\sum_{j=1}^{B_R} Q_n(x,r,\theta-\Omega_R t+2\pi j/B_R)\times e^{inB_F[(\Omega_R-\Omega_F)t-2\pi j/B_R]} \tag{14}$$

Again, the only knowledge of the source used is its symmetry properties. By writing Q_n as a Fourier series we find that the source term can be written as:

$$\sum_{n=-\infty}^{\infty}\sum_{m=-\infty}^{\infty} \hat{Q}_{n,m}(x,r)e^{i(nB_F-mB_R)\theta - i(nB_F\Omega_F - mB_R\Omega_R)t} \tag{15}$$

We thus find that the source and the solution can be written as a sum over n and m, the terms of which have frequency $nB_F\Omega_F - mB_R\Omega_R$ and a symmetry pattern with $|nB_F - mB_R|$ lobes. This symmetry pattern rotates with an angular frequency of $\dfrac{nB_F\Omega_F - mB_R\Omega_R}{nB_F - mB_R}$.

We now find for the complex amplitude of the corresponding tones:

$$\hat{p}_{n,m}(x,r) = \frac{i}{4}\int_{-\infty}^{\infty} e^{i\alpha x} H^{(2)}_{nB_F-mB_R}(\gamma r)\times \int_{r_h}^{R} \rho J_{nB_F-mB_R}(\gamma\rho)\tilde{Q}_{n,m}(\alpha,\rho)\,\mathrm{d}\rho\,\mathrm{d}\alpha \tag{16}$$

with γ determined by eq.(10) and $k = -(nB_F\Omega_F - mB_R\Omega_R)/c_0$. Note that for $m = 0$ or $n = 0$ we find the expression for the tones of the isolated front or rear rotor, see eq. (12).

In the next sections expression (16) will be used to analyse some general properties of contra-rotating propeller noise.

3 Applications

In the following examples a reference configuration is defined by:
$B_F = 11$
$B_R = 9$
$\Omega_F = 55$ rad/s
$\Omega_R = -60$ rad/s
$M = 0.25$
$R = 2$ m , both front and rear rotor
$r_h = 0.6$ m
$c_0 = 340$ m/s
$r = 10$ m, sideline observer distance
Examples will be given for this configuration and variations on the specified parameters.

3.1 Which tones can be expected

It is a well-known property of Bessel functions, that their value is small if the argument is much smaller than the order. Here we obtain high orders if n and m have opposite sign. For this situation the frequency of the interaction tone is a difference frequency, and will be relatively low. As the maximum value of γ can be shown to be proportional to the frequency, it can be expected from eq. (16) that these tones will not radiate efficiently. Indeed, in experiments only sum tones (i.e. n and m having equal sign) are observed, see e.g. [2].

3.2 Effect of spanwise source distribution

Firstly, the effect of the spanwise source distribution in the case of a single-rotating propeller is investigated. To this end the

quantity $\rho J_{nB}(\gamma_m \rho)$ is plotted in Figure 2 for $n = 1$ and various values of B. γ_m^2 is the maximum of γ^2. The values are normalized by the value at the tip.

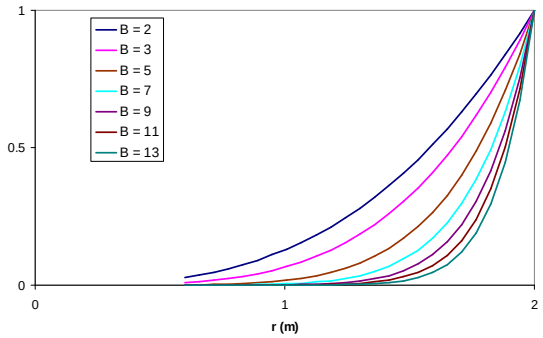

Fig. 2. Absolute value of $\rho J_B(\gamma_m \rho)$ (normalized) for various blade numbers.

From this figure it can be seen that the higher the blade number, the more the tip region is dominating, assuming that there are no very large variations in the source distribution. This conclusion was derived earlier by Parry and Crighton [3].

Secondly the interaction tones for a contra-rotating propeller will be investigated. For the reference case described above, the absolute value of $\rho J_j(\gamma_m \rho)$ is plotted in Figure 3, with $j = nB_F - mB_R$. Here the values are normalized to the maximum value of each curve.

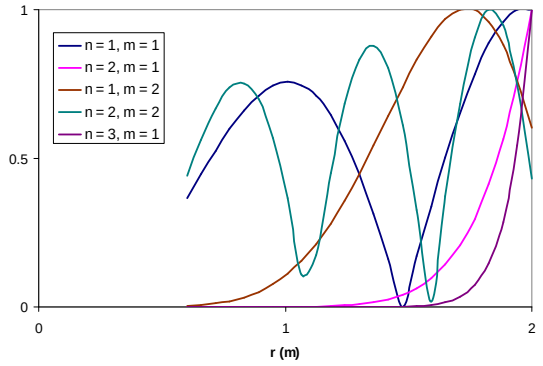

Fig. 3. Absolute value of $\rho J_j(\gamma_m \rho)$ (normalized) for various blade numbers, interaction tones.

For lower values of j the source values over the whole blade span will contribute. For the higher values of j it can be shown [4] that the region around $r = z^*R$ will dominate, where z^* is a called the 'Mach radius'. For $n = 1$, $m = 2$ this radius is smaller than the tip radius, for $n = 2$, $m = 1$ and $n = 2$, $m = 1$, z^* is larger than the tip radius. In the latter cases the tip region is dominating.

3.3 Directivity

In this section a constant source will be assumed: $\tilde{Q}_{n,m}(\alpha, \rho) = 1$, which amounts to a δ-function in x direction (only sources in the rotor plane) and a constant distribution in spanwise direction. In Figure 4 the values are shown for the rear rotor BPF tone ($n = 0$, $m = 1$) and the first interaction tone ($n = 1$, $m = 1$), normalized to their maximum value.

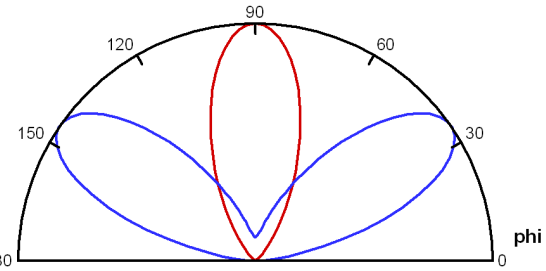

Fig. 4. Directivity of rear rotor BPF tone (red) and first interaction tone (blue).

This shape of the rotor alone tone directivity may be expected to be quite similar to that of the actual propeller: as shown above, this tone is dominated by the blade tip region and details of the source distribution are relatively unimportant. Somewhat more differences may be expected for the interaction tone directivity, in particular will the symmetry of pattern be broken if a realistic source distribution would be used. Nevertheless, a general difference between rotor alone tones and interaction tones is clearly illustrated by Figure 4: the radiation of rotor alone tones is restricted to the angles near the propeller plane, while the interaction tones radiate in the forward and rearward arc.

Note that this interaction tone does not radiate on the axis itself. In fact it can be shown mathematically that radiation on the axis itself is only possible if the order of the Bessel funcion is zero. For the reference case the lowest values of n and m for which this occurs are $n = 9$ and $m = 11$. However, it is unlikely that these high Fourier modes are excited very much. Instead,

the directivity of the n = 1, m = 1 tone is compared to that of the same case with 11 blades in the rear rotor, instead of 9, see Figure 5.

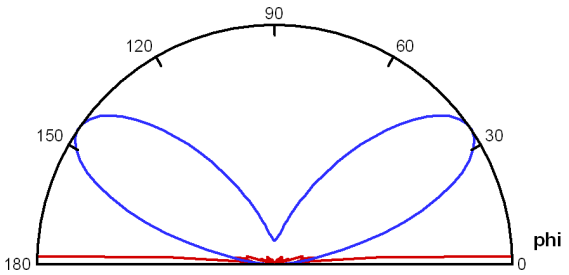

Fig. 5. Directivity of the n = 1, m = 1 interaction tone for B_F = 11 and B_R = 9 (blue) and 11 (red) respectively.

In the latter case the directivity is extremely concentrated on the x-axis. The nB_F - mB_R = 0 case thus generates a pressure field that is axi-symmetrically radiating along the axis, like that of a piston moving back and forth.

3.4 Extrapolation from near- to far-field

One of the most useful applications of the theory presented here, is the possibility to extrapolate far-field from near field-data.

Acoustic data from experiments are often obtained in an acoustically treated wind tunnel. Measurements at low speed can be carried out in a large test section, where microphones can be placed in the far-field. In high-speed wind tunnels, however, microphones are necessarily mounted close to the source, see e.g. [2]. Experimental acoustic data for cruise conditions are thus often only available in the near-field.

Data from computations, obtained from Computational Fluid Dynamics, are also restricted to the near-field, simply because it requires too much computation time and computer memory, if the computational domain is extended to the far-field.

The second line of the right hand side of eq. (16) contains all the information on the source, but no reference to the observer distance r. This enables us to write:

$$\hat{p}_n(x,r) = \frac{1}{2\pi}\int_{-\infty}^{\infty} e^{i\alpha x}\frac{H_{nB}^{(2)}(\gamma r)}{H_{nB}^{(2)}(\gamma r_0)}\int_{-\infty}^{\infty} e^{-i\alpha\xi}\hat{p}_n(\xi,r_0)\,\mathrm{d}\xi\,\mathrm{d}\alpha \qquad (17)$$

where r_0 is arbitrary, but larger than R. If the complex pressure amplitude of a tone is known on a near-field sideline in sufficient detail, such that its Fourier transform in axial direction can be taken, the pressure amplitude can be computed at any other distance outside the propeller disk. Note that in eq. (17) no assumptions have been made on the source.

Unfortunately no contra-rotating noise data are available in the public domain to demonstrate this extrapolation procedure. However, at NLR data are available of the single-rotating, 6-bladed, Fokker 50 propeller, which was tested in the DNW-LLF wind tunnel. In Figure 6 the measured noise levels of the BPF tone is plotted as a function of axial coordinate, at two sideline distances: r = 1.32R and r = 3.9R. The data at 1.32R were used as input, and extrapolated to 3.9R, presented as the solid line.

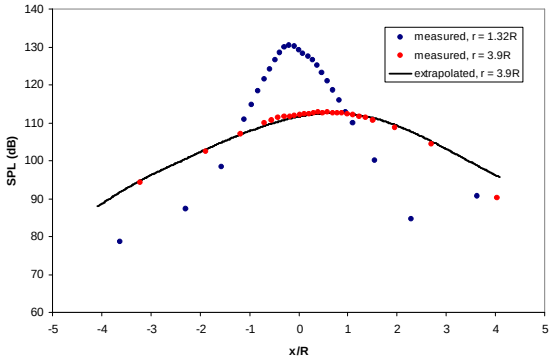

Fig. 6. Application of the extrapolation method to noise data of the Fokker 50 propeller.

The agreement is typically within 1 dB. Note that if simply proportionality with distance would have been assumed, as may be done in the far field, the peak level would decrease by only 9.4 dB, instead of 18 dB shown here.

Eq. (17) can also be used in principle to obtain near-field results from far-field data, similar to the technique of acoustic holography. However, some care should be taken regarding the numerical implementation. With M < 1, we

find that the radial wavenumber γ only assumes real values for a finite part of the α-domain, i.e. in the interval:

$$\begin{aligned} \frac{-k}{1+M} \le \alpha \le \frac{k}{1-M}, \quad k>0 \\ \frac{k}{1-M} \le \alpha \le \frac{-k}{1+M}, \quad k<0 \end{aligned} \tag{18}$$

For the remaining part of the α-domain γ has a negative imaginary value, which corresponds to evanescent waves, which decay exponentially with increasing r. However, using eq.(17) to compute near-field acoustic pressures from far-field data, numerical or experimental inaccuracies will excite spurious evanescent waves which grow exponentially in the direction towards the source, and the method will yield unphysically high values for the near field pressure perturbation. Therefore, in the numerical implementation of eq.(17), the integration over α should be restricted to the interval given by eq. (18), i.e. incorporating only propagating waves, which means that part of the near-field pressure will not be recovered.

4 Conclusions

Analytical expressions have been derived for the radiation of noise from single- and contra-rotating propellers. These expressions are independent of a detailed source description.

It is shown that these expressions can be used to

- assess which tones can be expected to appear in a measured noise spectrum,
- assess the effect of spanwise source distribution,
- analyze the directivity of the individual noise components.

Furthermore, it is shown how the mathematical model enables an exact extrapolation of near-field noise data to the far field.

References

[1] Schulten, J.B.H.M. *Sound generation by ducted fans and propellers as a lifting surface problem* Ph. D. Thesis, University of Twente, ISBN 90-9005714-5, 1993.

[2] Dittmar, J.H. and Stang, D.B. *Noise reduction for model counterrotation propeller at cruise by reducing aft-propeller diameter* NASA-TM-88936, 1987.

[3] Parry, A.B and Crighton, D.G. Asymptotic theory of propeller noise – Part I: Subsonic single-rotation propeller. *AIAA Journal*, Vol. 27, pp 1184 – 1190, 1989.

[4] Parry, A.B. and Crighton, D.G. Prediction of counter-rotation propeller noise. *AIAA 12th Aeroacoustics Conference*, 10-12 April 1989, San Antonio, TX, AIAA 89-1141, 1989.

Contact Author Email Address

brouwer@nlr.nl

Copyright Statement